Journal of Magnetism and Magnetic Materials 385 (2015) 277–281

Contents lists available at ScienceDirect

Journal of Magnetism and Magnetic Materials

journal homepage: www.elsevier.com/locate/jmmm

Crystallization behavior and magnetic properties in High Fe content FeBCSiCu alloy system

X.D. Fan *, B.L. Shen *

School of Materials Science and Engineering, Southeast University, Nanjing 211189, PR China

ARTICLE INFO

Article history:
Received 7 January 2015
Received in revised form
4 March 2015
Accepted 8 March 2015
Available online 9 March 2015

Keywords:
Soft magnetic material
Glass-forming ability
Fe-based nanocrystalline alloy
High saturation magnetic flux density

ABSTRACT

High Fe content FeBCSiCu nanocrystalline alloys are prepared by annealing melt-spun amorphous ribbons with aim at increasing saturation magnetic flux density. Microstructures identified by XRD and TEM reveal that Cu addition inhibits the surface crystallization of $Fe_{86}B_7C_7$ alloy and improve its glass-forming ability. Activation energy of crystallization calculated by Kissinger's equation indicates that both Cu and Si addition promotes the precipitation of α-Fe phase and improves the thermal stability. VSM and *DC B–H* loop tracer measurements show that the $Fe_{85.5}B_7C_6Si_1Cu_{0.5}$ nanocrystalline alloy exhibits high saturation magnetic flux density of 1.8 T and low coercivity of 10 A/m, respectively. *AC* properties measured by *AC B–H* analyzer show this alloy exhibits low core loss of 0.35 W/kg at 1 T at 50 Hz. Low material cost and convenient productivity make the $Fe_{85.5}B_7C_6Si_1Cu_{0.5}$ nanocrystalline alloy an economical application in industry.

1. Introduction

Nanocrystalline soft magnetic alloys [1–4] produced by crystallizing amorphous phases have attracted great attention due to their excellent soft magnetic properties such as high saturation magnetic flux density (B_s), high effective permeability (μ_e), low coercivity (H_c) and low core loss (P). And the development and application of nanocrystalline soft magnetic materials have greatly contributed to the development of electronics and power industry, especially for energy saving. Since the first nanocrystalline alloy with nominal composition of $Fe_{73.5}Si_{13.5}B_9Nb_3Cu_1$ was found by Yoshizawa [1] in 1988, after 20 years of development, nanocrystalline alloy systems mainly include FeSiBNbCu [1], FeZrBCu [2] and FeCoZrBCu [3] patented under the trade name of FINEMET, NANOPERM and HITPERM, respectively. For years, scientists made a thorough and systematic study on existing nanocrystalline alloy system to explain the original of excellent soft magnetic properties, in order to establish the crystallization mechanism and realize magnetic properties control [5–13]. Then, on the basis of the above theoretical research, many kinds of nanocrystalline soft magnetic alloys were subsequently synthesized such as FeBCu [14,15], FeSiBPCu [16–18], FePCCu [19], FePCu [20] and FeNbBCu [21]. However, these alloys contained either precious metal element Nb or more than 14% of the expensive element B, which increases the material cost, or contained volatile element P, the composition is difficult to precisely control, thus limited their application.

Accordingly, we synthesized the $Fe_{84-x}B_{10}C_6Cu_x$ nanocrystalline alloys [22,23] with good soft magnetic properties, low cost, as well as easy production. But compared with FeBCu and FeSiBPCu, the $Fe_{84-x}B_{10}C_6Cu_x$ nanocrystalline alloys exhibit a rather low B_s. It is well known that Cu addition can promote the precipitation of α-Fe particle thus increase the B_s, and Si substitution can inhibit the Fe–B compounds, increase the thermal stability, which is benefit for magnetic properties. So in this paper, with the aim at increasing B_s and improving the soft magnetic properties, high Fe content $Fe_{86}B_7C_7$, $Fe_{85.5}B_7C_7Cu_{0.5}$ and $Fe_{85.5}B_7C_6Si_1Cu_{0.5}$ alloys were developed. And the effect of Cu and Si addition on glass-forming ability, thermal stability, microstructures and magnetic properties in FeBCSiCu alloy system was discussed.

2. Experimental procedures

Alloy ingots with nominal compositions of $Fe_{86}B_7C_7$, $Fe_{85.5}B_7C_7Cu_{0.5}$ and $Fe_{85.5}B_7C_6Si_1Cu_{0.5}$ were prepared by arc melting the mixtures of Fe (99.99 mass%), B (99.5 mass%), Si (99.99 mass%), Cu (99.99 mass%) and pre-alloyed Fe–C alloy under a high purified argon atmosphere. Each ingot was melted five times to ensure compositional homogeneity. Amorphous ribbons were prepared by single roller melt spinning with linear velocity of 40 m/s. The width and thickness were 1 mm and 20 μm,

* Corresponding authors. Fax: +86 25 52091077.
E-mail addresses: fanxd@seu.edu.cn (X.D. Fan), blshen@seu.edu.cn (B.L. Shen).

http://dx.doi.org/10.1016/j.jmmm.2015.03.033
0304-8853/

respectively. Melt-spun ribbons were annealed to develop nanocrystalline. The annealing was carried out by keeping the ribbons in the tubular furnace preheated to annealing temperature for the preset annealing time in argon atmosphere followed by water quenching cooling. Microstructures were identified by X-ray diffraction (XRD) with Cu $K\alpha_1$ radiation, transmission electron microscopy (TEM) and selected area electron diffraction (SAED). Thermal stability was evaluated by differential scanning calorimeter (DSC). B_s and H_c under a maximum applied field of 800 kA/m and 1 kA/m were measured by a vibrating sample magnetometer (VSM) and a *DC B–H* loop tracer, respectively. The melt-spun ribbons were wound into laminated toroids with 10 mm in outer diameter, 6 mm in inner diameter, subsequently isothermal annealed in the same condition with the ribbon specimens in order to determine the *AC* properties. Core losses at 1 T and 50 Hz, 400 Hz and 1 kHz were measured with an *AC B-H* analyzer.

3. Results and discussion

3.1. Microstructures of melt-spun alloys

Fig. 1 shows the XRD patterns of $Fe_{86}B_7C_7$, $Fe_{85.5}B_7C_7Cu_{0.5}$ and $Fe_{85.5}B_7C_6Si_1Cu_{0.5}$ melt-spun ribbons, all samples are measured by free surface. It can be obviously seen that two sharp crystallization peaks identified to Fe_3C phase exist for $Fe_{86}B_7C_7$ alloy. To understand this crystallization behavior, further XRD examination is taken by both free surface and wheel surface. As shown by the inset in Fig. 1, the pattern of wheel surface shows only broad peak, indicating the formation of single amorphous phase. It is not difficult to understand that the cooling rate of free surface is lower than the wheel surface, resulting in a surface crystallization behavior. But with the addition of Cu and Si, the crystallization peak disappears and the sample exhibits halo patterns, indicating the amorphous structure. Fig. 2 shows the HRTEM image and SAED pattern of $Fe_{85.5}B_7C_7Cu_{0.5}$ melt-spun ribbon. The HRTEM image reveals that the microstructure of the alloy exhibits long-range disorder. And the SAED pattern shows diffused diffraction rings and no existence of spots corresponding to any crystalline phase, indicating that the $Fe_{85.5}B_7C_7Cu_{0.5}$ alloy is of completely amorphous structure, which is in agreement with the XRD results. Hence, the microstructure analysis results indicated that Cu addition inhibits the surface crystallization of $Fe_{86}B_7C_7$ alloy and improves its glass-forming ability. This phenomenon is consistent with the completive principle reported by Johnson [24], who pointed out that the nucleation of different crystallization phase competes with each other and makes the supercooled liquid reach a relatively stable state, which is conducive to the formation of amorphous. According to the former results [23], Cu addition promoted the precipitation of α-Fe phase in the FeBCCu alloy system, the competitive formation of Fe_3C, α-Fe and amorphous phase can drastically impede the devitrification, which is benefit for amorphous forming.

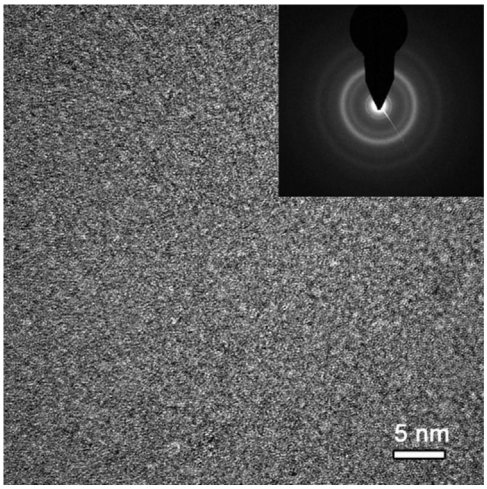

Fig. 2. HRTEM image and SAED pattern of $Fe_{85.5}B_7C_7Cu_{0.5}$ melt-spun ribbon.

3.2. Thermal stability and crystallization behaviors

The DSC curves for $Fe_{86}B_7C_7$, $Fe_{85.5}B_7C_7Cu_{0.5}$ and $Fe_{85.5}B_7C_6Si_1Cu_{0.5}$ melt-spun ribbons are showed in Fig. 3. It can be seen that the crystallization process includes two stages. According to former research results [23], it has been confirmed that the first crystallization onset temperature (T_{x1}) and the second one (T_{x2}) represent the precipitation temperature of a-Fe phase and Fe–B compounds, respectively. But unlike the $Fe_{84-x}B_{10}C_6Cu_x$ alloy system, the T_{x1} of $Fe_{85.5}B_7C_7Cu_{0.5}$ alloy occurs at 349 °C, which is higher than the $Fe_{86}B_7C_7$ alloy (345 °C). The $Fe_{85.5}B_7C_6Si_1Cu_{0.5}$ alloy exhibits a slightly lower T_{x1} compared to $Fe_{85.5}B_7C_7Cu_{0.5}$ sample, but T_{x2} increases dramatically from 470 °C to 505 °C. Thus the temperature difference (ΔT_x) between T_{x1} and T_{x2} expands, reflecting that the $Fe_{85.5}B_7C_6Si_1Cu_{0.5}$ alloy exhibits a better thermal stability, which is advantageous for synthesizing nanocrystalline alloy with good soft magnetic properties. As the large temperature interval advantages the formation of soft magnetic α-Fe nanocrystalline phase without any precipitation of nonferromagnetic phases, which deteriorates the softness of the alloys [25,26].

In order to investigate the dynamics of crystallization process, a crystallization activation energy measurement with different heating rate of 10, 20, 30 and 40 °C/min is carried out. Activation

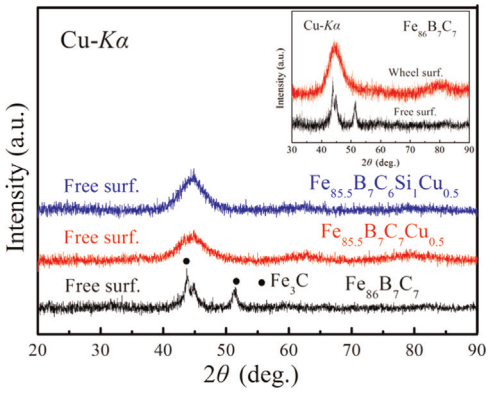

Fig. 1. XRD patterns of $Fe_{86}B_7C_7$, $Fe_{85.5}B_7C_7Cu_{0.5}$ and $Fe_{85.5}B_7C_6Si_1Cu_{0.5}$ melt-spun ribbons.

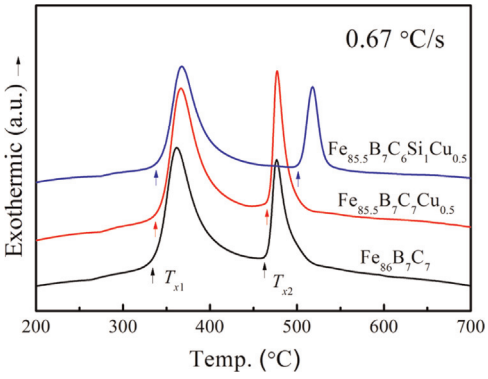

Fig. 3. DSC curves for $Fe_{86}B_7C_7$, $Fe_{85.5}B_7C_7Cu_{0.5}$ and $Fe_{85.5}B_7C_6Si_1Cu_{0.5}$ melt-spun ribbons.

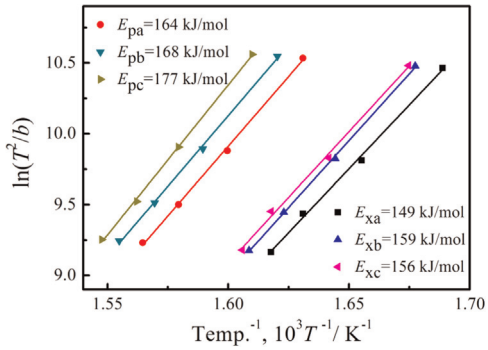

Fig. 4. Kissinger plots of (a) $Fe_{86}B_7C_7$, (b) $Fe_{85.5}B_7C_7Cu_{0.5}$ and (c) $Fe_{85.5}B_7C_6Si_1Cu_{0.5}$ alloys.

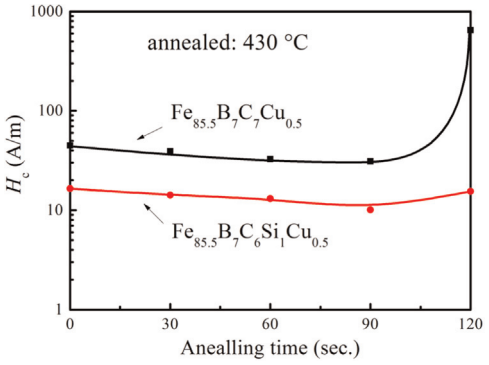

Fig. 5. The dependence of H_c on annealing time for $Fe_{85.5}B_7C_7Cu_{0.5}$ and $Fe_{85.5}B_7C_6Si_1Cu_{0.5}$ alloys.

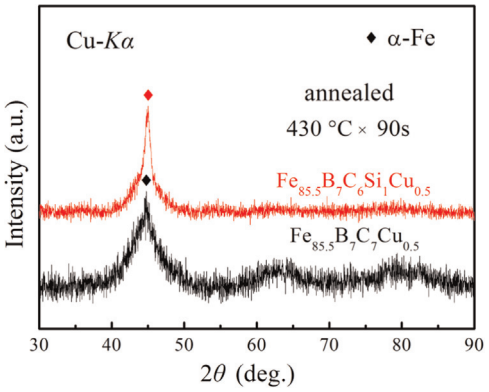

Fig. 6. XRD patterns of $Fe_{85.5}B_7C_7Cu_{0.5}$ and $Fe_{85.5}B_7C_6Si_1Cu_{0.5}$ alloy ribbons annealed at 430 °C for 90 s.

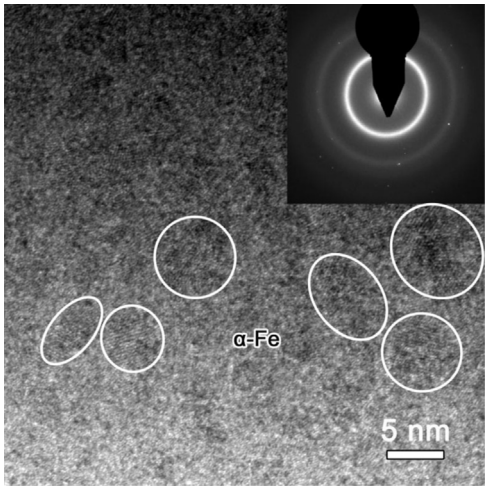

Fig. 7. HRTEM image and SAED pattern of $Fe_{85.5}B_7C_7Cu_{0.5}$ alloy annealed at 430 °C for 90 s.

energy of both exothermic peaks can be calculated by the Kissinger's equation [27].

$$\ln\left(\frac{T^2}{\beta}\right) = \ln\left(\frac{E_a}{R}\right) - \ln\nu + \frac{E_a}{RT} \quad (1)$$

Where β is the heating rate, E_a is the activation energy, ν is the frequency factors and R is gas constant. Fig. 4 shows the Kissinger plots of $\ln(T^2/\beta)$ versus $1/T$ for (a) $Fe_{86}B_7C_7$, (b) $Fe_{85.5}B_7C_7Cu_{0.5}$ and (c) $Fe_{85.5}B_7C_6Si_1Cu_{0.5}$ alloys. Where the symbols E_{xa}–E_{xc} and E_{pa}–E_{pc} stand for Kissinger plots corresponding to the crystallization onset temperature and the peak temperature of the first exothermic peak for the selected composition alloys, respectively. Accordingly, the apparent activation energy can be calculated through the slope of E_a/R, as marked in the figure.

As it is well known, the crystallization onset temperature is considered to be associated with the nucleation process, and the peak temperature is with the growth process. Therefore, the activation energy deduced from the crystallization onset temperatures and the peak temperatures correspond to nucleation and growth, respectively [28,29]. According to the result, the value of E_x for the selected alloys is lower than that of E_p, implying that the nucleation processes are easier than the growth processes. The E_x of $Fe_{85.5}B_7C_7Cu_{0.5}$ alloy is 159 k J/mol, which is higher than that of $Fe_{86}B_7C_7$ alloy (149 k J/mol). The result indicates that Cu addition makes nucleation harder, hence improves the glass-forming ability. The $Fe_{85.5}B_7C_6Si_1Cu_{0.5}$ alloy exhibits a maximum E_p of 177 k J/mol, implying that Si substitution makes nucleation growth more difficult, and hence improves its thermal stability.

3.3. Microstructures and magnetic properties of nanocrystalline alloys

A series of annealing temperature (T_a) range from 370 °C to 450 °C were selected for FeBCSiCu alloy system. It was found that H_c exhibited a minimum value near 430 °C. So the proper T_a was finally fixed at 430 °C. Fig. 5 shows the dependence of H_c on annealing time (t) for $Fe_{85.5}B_7C_7Cu_{0.5}$ and $Fe_{85.5}B_7C_6Si_1Cu_{0.5}$ alloys. Here the values of H_c are calculated by averaging three specimens annealed in the same condition. It is seen that for both alloys, H_c decreases gradually and reaches the minimum at t=90 s. After that, the H_c of $Fe_{85.5}B_7C_7Cu_{0.5}$ alloy increases rapidly as t increases. While for $Fe_{85.5}B_7C_6Si_1Cu_{0.5}$ alloy, H_c shows a slow increasing trend due to the better thermal stability. According to the result, we determined t as 90 s.

Fig. 6 shows the XRD patterns of $Fe_{85.5}B_7C_7Cu_{0.5}$ and $Fe_{85.5}B_7C_6Si_1Cu_{0.5}$ alloy ribbons annealed at 430 °C for 90 s. As a result, a crystalline phase identified as α-Fe superimposes on that of the amorphous phase for $Fe_{85.5}B_7C_7Cu_{0.5}$ alloy. But the diffraction intensity is weak and the volume fraction of crystalline phase is small, so the grain size cannot be estimated. For further understanding the microstructure, TEM and SEAD analyses are carried out for $Fe_{85.5}B_7C_7Cu_{0.5}$ annealed alloy. The result is showed in Fig. 7. The HRTEM image reveals that the microstructure consists of residual amorphous phase and α-Fe grain that is embedded in the amorphous matrix phase. The grain size is from 5 to 10 nm. The SAED pattern shows only a few spots scatter in the diffraction rings, indicating the precipitation of α-Fe nanocrystals is small, which is consistent with the XRD result. As for the $Fe_{85.5}B_7C_6Si_1Cu_{0.5}$ annealed alloy, obvious crystalline peak corresponding to (110) α-Fe phase is detected. The grain size estimated on Scherrer's equation is 15 nm and the volume fraction of

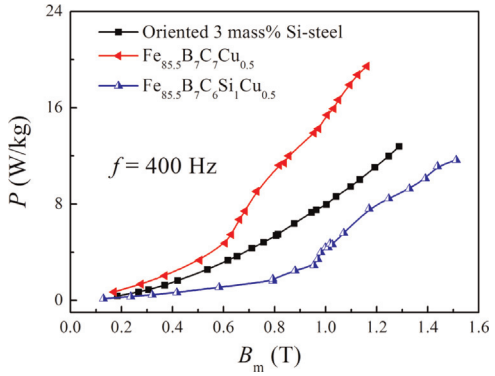

Fig. 8. The dependence of core loss (P) on maximum magnetic flux density (B_m) for $Fe_{85.5}B_7C_7Cu_{0.5}$ and $Fe_{85.5}B_7C_6Si_1Cu_{0.5}$ nanocrystalline alloys at 400 Hz, together with that of a toroidal core of oriented 3 mass% Si-steel.

Table 1
Magnetic properties of $Fe_{85.5}B_7C_7Cu_{0.5}$ and $Fe_{85.5}B_7C_6Si_1Cu_{0.5}$ nanocrystalline alloys under several conditions are compared with those of $Fe_{83}B_{10}C_6Cu_1$, $Fe_{73.5}Cu_1Nb_3Si_{13.5}B_9$, $Fe_{83.7}Cu_{1.5}B_{14.8}$ and $Fe_{83.3}Si_4B_8P_4Cu_{0.7}$ nanocrystalline alloys and commercial oriented 3 mass% Si-steel.

Alloys	B_s (T)	H_c (A/m)	$P_{10/50}$ (W/kg)	$P_{10/400}$ (W/kg)	$P_{10/1k}$ (W/kg)
$Fe_{85.5}B_7C_7Cu_{0.5}$	1.81	30	1.08	14.4	42.3
$Fe_{85.5}B_7C_6Si_1Cu_{0.5}$	1.80	10	0.35	4.4	14.6
$Fe_{83}B_{10}C_6Cu_1$ [23]	1.78	5	0.34	4.3	12.5
$Fe_{73.5}Cu_1Nb_3Si_{13.5}B_9$ [1]	1.24	0.53	$P_{2/20k}$ =2.1		
$Fe_{83.7}Cu_{1.5}B_{14.8}$ [14]	1.82	7	$P_{15/50}$ =0.38		
$Fe_{85}Si_2B_8P_4Cu_1$ [18]	1.85	6	$P_{15/50}$ =0.39		
Oriented 3 mass% Si-steel [30,31]	2.03	8	0.41	7.9	27.1

crystalline phase calculated from {110} plane is about 15%. Hence, the addition of both Cu and Si promotes the precipitation of α-Fe phase and leads to a fine nanostructure. That can be explained by the reason that the activation energy of nucleation for $Fe_{85.5}B_7C_6Si_1Cu_{0.5}$ alloy is 156 k J/mol, which is lower than that of $Fe_{85.5}B_7C_7Cu_{0.5}$ alloy. The lower apparent activation energy makes the nucleation of α-Fe easier. Meanwhile, Si substitution improves the thermal stability of the alloy, which is beneficial for homogeneous precipitation of α-Fe nanocrystals without fast growth.

Fig. 8 shows the dependence of core loss (P) on maximum magnetic flux density (B_m) for $Fe_{85.5}B_7C_7Cu_{0.5}$ and $Fe_{85.5}B_7C_6Si_1Cu_{0.5}$ nanocrystalline alloys at 400 Hz, together with that of a toroidal core of oriented 3 mass% Si-steel. Here the Si-steel used for comparison is the conventional grain-oriented (CGO) steel with 0.23 mm in thickness. Due to the high H_c, $Fe_{85.5}B_7C_7Cu_{0.5}$ alloy exhibits high P and a fast increasing trend as B_m increased. However, the $Fe_{85.5}B_7C_6Si_1Cu_{0.5}$ alloy exhibits obviously lower H_c and P according to the homogeneous precipitation of α-Fe grain, which decreases the overall magnetocrystalline anisotropy. What is more, the increasing rate of P against B_m for this nanocrystalline alloy is small even when $B_m > 1$ T, which means the $Fe_{85.5}B_7C_6Si_1Cu_{0.5}$ alloy can be used in high magnetic flux density and frequency.

Table 1 lists the B_s, H_c and P of $Fe_{85.5}B_7C_7Cu_{0.5}$ and $Fe_{85.5}B_7C_6Si_1Cu_{0.5}$ nanocrystalline alloys under several conditions are compared with those of $Fe_{83}B_{10}C_6Cu_1$ [23], $Fe_{73.5}Cu_1Nb_3Si_{13.5}B_9$ [1], $Fe_{83.7}Cu_{1.5}B_{14.8}$ [14] and $Fe_{85}Si_2B_8P_4Cu_1$ [18] nanocrystalline alloys and commercial oriented 3 mass% Si-steel [30,31]. Here, the symbols $P_{10/50}$, $P_{10/400}$ and $P_{10/1k}$ stand for core losses at 1 T at 50 Hz, 400 Hz and 1 kHz, respectively. It can be seen that compared with $Fe_{83}B_{10}C_6Cu_1$ alloy, this alloy system exhibits a higher B_s due to the higher Fe content and precipitation of α-Fe grain. The value of B_s is 1.81 T for $Fe_{85.5}B_7C_7Cu_{0.5}$, which is as high as that of $Fe_{83.7}Cu_{1.5}B_{14.8}$ alloy and much higher than that of $Fe_{73.5}Cu_1Nb_3Si_{13.5}B_9$ alloy. But the H_c is as high as 30 A/m, though the grain size D of the alloy is small (5–10 nm). The result seems to be inconsistent with Herzer's random anisotropy model [5,6], which proposed the increasing rate of H_c is almost proportional to D^6 in nanocrystalline alloy systems. The reason is that the volume fraction of crystalline phase is too low to decrease the overall magnetocrystalline anisotropy, for high density α-Fe nanocrystals are required for strong magnetic exchange coupling, which is necessary to average out the magnetocrystalline anisotropy [13,32]. And former research result has confirmed that magnetoelastic anisotropy determined by mangetostriction and stress also has an effect on the coercivity [20]. As for the $Fe_{85.5}B_7C_6Si_1Cu_{0.5}$ nanocrystalline alloy, the addition of both Cu and Si has promoted the precipitation of α-Fe phase and made the alloy a fine microstructure. Therefore, the overall magnetocrystalline anisotropy is effectively decreased and thus, the alloy exhibits a much lower H_c of 10 A/m. What is more, the $Fe_{85.5}B_7C_6Si_1Cu_{0.5}$ nanocrystalline alloy also exhibits a high B_s of 1.8 T, low core loss $P_{10/50}$ of 0.35 W/kg, which is about 85% that of oriented 3 mass% Si-steel. And the advantage of core losses at higher frequencies, such as $P_{10/400}$ and $P_{10/1k}$, compared to those of commercial oriented Si-steel is obvious. What is more, the low material cost and convenient productivity because of not-containing easily-oxidized metal elements or volatile elements make this nanocrystalline alloy an economical application in industry.

4. Conclusions

In conclusion, high Fe content FeBCSiCu alloy system with selected composition of $Fe_{86}B_7C_7$, $Fe_{85.5}B_7C_7Cu_{0.5}$ and $Fe_{85.5}B_7C_6Si_1Cu_{0.5}$ alloy is investigated. It is found that Cu addition inhibits the surface crystallization and improves the glass-forming ability of $Fe_{86}B_7C_7$ alloy. While Si substitution promotes the precipitation of Fe–B compounds and improves the thermal stability in $Fe_{85.5}B_7C_6Si_1Cu_{0.5}$ alloy. The result is finely in agreement with the crystallization activation energy investigation, as the $Fe_{85.5}B_7C_6Si_1Cu_{0.5}$ alloy has a maximum E_p of 177 kJ/mol. The addition of both Cu and Si also promotes the precipitation of α-Fe phase and makes the alloy a fine microstructure. Therefore, the $Fe_{85.5}B_7C_6Si_1Cu_{0.5}$ nanocrystalline alloy exhibits excellent magnetic properties such as high B_s of 1.8 T, low H_c of 10 A/m and low $P_{10/50}$ of 0.35 W/kg.

Acknowledgements

This work was supported by the National Natural Science Foundation of China (Grant nos. 51401052, 51271194 and 51471050), Jiangsu Planned Projects for Postdoctoral Research Funds (Grant no. 1302044B) and the Fundamental Research Funds for the Central Universities (Grant no. 3212004602).

References

[1] Y. Yoshizawa, S. Oguma, K. Yamauchi, J. Appl. Phys. 64 (1988) 6044.
[2] K. Suzuki, A. Makino, N. Kataoka, A. Inoue, T. Masumoto, Mater. Trans. JIM 32 (1991) 93.
[3] K. Suzuki, A. Makino, A. Inoue, T. Masumoto, J. Appl. Phys. 70 (1991) 6232.
[4] M.A. Willard, D.E. Laughlin, M.E. McHenry, J. Appl. Phys. 84 (1998) 6773.
[5] G. Herzer, IEEE Trans. Magn. 26 (1990) 1397.
[6] G. Herzer, J. Magn. Magn. Mater. 112 (1992) 258.

[7] K. Hono, Y. Zhang, A. Inoue, Mater. Trans. JIM 36 (1995) 909.
[8] M. Ohnuma, K. Hono, H. Onodera, Nanostruct. Mater. 12 (1999) 693.
[9] K. Hono, D.H. Ping, M. Ohnuma, H. Onodera, Acta Mater. 47 (1999) 997.
[10] M.E. McHenry, D.E. Laughlin, Acta Mater. 48 (2000) 223.
[11] M.E. McHenry, F. Johnson, H. Okumura, T. Ohkubo, V.R.V. Ramanan, D. E. Laughlin, Scr. Mater. 48 (2003) 881.
[12] K. Suzuki, G. Herzer, Scr. Mater. 67 (2012) 548.
[13] G. Herzer, Acta Mater. 61 (2013) 718.
[14] M. Ohta, Y. Yoshizawa, Jpn. J. Appl. Phys. 46 (2007) L477.
[15] M. Ohta, Y. Yoshizawa, Appl. Phys. Lett. 91 (2007) 062517.
[16] A. Makino, H. Men, T. Kubota, K. Yubuta, A. Inoue, Mater. Trans. 50 (2009) 204.
[17] A. Makino, H. Men, K. Yubuta, T. Kubota, J. Appl. Phys. 105 (2009) 013922.
[18] P. Sharma, X. Zhang, Y. Zhang, A. Makino, J. Appl. Phys. 15 (2014) 17A340.
[19] Y.L. Jin, X.D. Fan, H. Men, X.C. Liu, B.L. Shen, Sci. China Technol. Sci. 55 (2012) 3419.
[20] F.G. Chen, Y.G. Wang, X.F. Miao, H. Hong, K. Bi, J. Alloys Compd. 549 (2013) 26.
[21] L. Xue, H.S. Liu, L.T. Dou, W.M. Yang, C.T. Chang, A. Inoue, X.M. Wang, R.W. Li, B. L. Shen, Mater. Des. 56 (2014) 227.
[22] X.D. Fan, A.B. Ma, H. Men, G.Q. Xie, B.L. Shen, A. Makino, A. Inoue, J. Appl. Phys. 109 (2011) 07A314.
[23] X.D. Fan, H. Men, A.B. Ma, B.L. Shen, J. Magn. Magn. Mater. 326 (2013) 22.
[24] W.L. Johnson, MRS Bull. 24 (1999) 42.
[25] A. Makino, A. Inoue, T. Masumoto, Mater. Trans. JIM 36 (1995) 924.
[26] B.L. Shen, H. Kimura, A. Inoue, Mater. Trans. JIM 43 (2002) 589.
[27] H.E. Kissinger, Anal. Chem. 29 (1957) 1702.
[28] F.X. Qin, H.F. Zhang, B.Z. Ding, Z.Q. Hu, Intermetallics 12 (2004) 1197.
[29] L.Y. Cui, H. Men, A. Makino, T. Kubota, K. Yubuta, M. Qi, A. Inoue, Mater. Trans. 11 (2009) 2515.
[30] D.F. Binns, A.B. Crompton, A. Jaberansari, IEEE Proc. Part C: Gen. Transm. Distrib. 133 (1986) 451.
[31] M. Abe, Y. Takada, T. Murakami, Y. Tanaka, Y. Mihara, J. Mater. Eng. 11 (1989) 109.
[32] Z. Akase, S. Aizawa, D. Shindo, P. Sharma, A. Makino, J. Magn. Magn. Mater. 375 (2015) 10.